Computer Mechanics Laboratory

Technical Report No. 95-009

Numerical Study of a Slider's Contact Take-off Process

by

Yong Hu and D.B. Bogy

Department of Mechanical Engineering
University of California
Berkeley, CA 94720

August 1995

Numerical Study of a Slider's Contact Take-off Process

Yong Hu and David. B. Bogy
Computer Mechanics Laboratory
Department of Mechanical Engineering
University of California
Berkeley, CA94720

Abstract

A mixed lubrication model is presented for predicting the effects of the air bearing and other design parameters on a slider's contact take-off performance. The Fukui-Kaneko linearized Boltzmann equation is used to model the nonlinear rarefaction effects in the modified Reynolds equation for the ultra-low fly height throughout the various stages of contact. An elastic-plastic asperity-based contact model is employed to extract the slider/disk contact forces and moments during the take-off process. The criterion for a slider to separate from a disk is defined as a certain percent of the loading force provided by the suspension. A sub-25nm shaped-rail slider is used in this study. The effects of the slider's crown, camber, twist, taper angle, as well as the disk's surface roughness and friction coefficient on the take-off velocity, fly height and other initial flying characteristics are studied. Among the many air bearing and other design parameters affecting the take-off velocity, the slider's crown and disk surface roughness are the most significant. Larger crowns and smoother disk surfaces lower the take-off velocity. The initial take-off flying characteristics are mostly determined by the slider's crown and the contact friction coefficient. Smaller crowns and friction coefficients produce a smoother initial take-off performance.

1 Introduction

In the ongoing effort to increase the storage capacity of magnetic hard disk drives, the drive manufacturers have reduced the head-disk spacing to the current level of about 65nm. The spacing in new designs is being reduced continually, and it is expected soon to reach sub-25nm levels. This trend towards lower fly heights puts increased demands on the mechanical durability of the head-disk interface during the contact start/stop (CSS) operation. CSS is a process in which the slider is in sliding contact with the disk as it starts and stops rotating. Therefore, minimizing mechanical wear during the CSS process is one of the essential design requirements. To meet the demands of these higher performance drives, designers must have a thorough understanding of the slider/disk interaction dynamics during the CSS process.

Two key parameters that characterize the mechanical durability of the CSS operation are the take-off velocity (TOV) and landing velocity (LV). With a higher TOV and LV, the sliding distance between the slider and disk is longer and the wear volume is larger. Methods of decreasing the TOV and LV have been pursued to reduce wear during the CSS operation. Lee et al. (1989) showed by use of strain gage transducers that the stiction and the TOV depend on the crown and rail width of the slider. Zhu and Bogy (1989) found that negative crown on the rails produces more disk wear than positive crown. They also explained the motion of crowned sliders during the CSS operation, where it is generally accepted that the slider initially pitches forward during take-off for positive crown sliders, but not for negative crown sliders. Suk et al. (1992) investigated the influence of crown on slider dynamics during the take-off stages of disk drives using the multi-channel laser interferometer. They concluded that positive crown sliders are less susceptible to undesirable disturbances caused by surface defects, and positive crown sliders may cause less disk wear due to their shorter sliding distance and less probability of point contacts with the disk in the initial stage of the take-off process. For comparison with the above-mentioned experimental investigation, there are very limited numerical studies of the slider's contact take-off/landing process due to the lack of a reliable model. Bolasna (1990) used an air bearing simulation to analyze the effects of slider/suspension parameters on the TOV of a taper

flat slider and a shaped IBM 3380 K slider. In his study, the actual slider/disk contact is ignored, and take-off from the disk is assumed to take place at a given fly height. Using this criterion, he found that crown is the most significant slider/suspension parameter affecting the TOV.

The goal of the present study is to investigate the effect of the air bearing and other design parameters on the slider's take-off process using a newly developed mixed lubrication model. The Fukui-Kaneko linearized Boltzmann equation is used to model the nonlinear rarefaction effects in the modified Reynolds equation for the ultra-low fly heights in CSS. An elastic-plastic asperity-based contact model (Chang, et al., 1987) is employed to extract the slider/disk contact forces and moments during the take-off process. We use a pre-defined percent of the suspension load as a criterion to determine a slider's take-off from a disk. A sub-25 nm slider with shaped-rails is used in this study. We present a simulation analysis of the effects of the slider's crown, camber, twist , taper angle, as well as the disk surface roughness and friction coefficient on the take-off velocity, the take-off fly height, and the initial flying characteristics. It is concluded that the slider's crown and disk surface roughness are the most significant parameters affecting the take-off velocity. Larger crowns and smoother disk surfaces reduce the take-off velocity. The initial take-off flying characteristics are mostly determined by the slider's crown and the contact friction coefficient. Smaller crowns and friction coefficients produce a smoother initial take-off performance.

2 Numerical Models

2.1 Generalized Reynolds Equation. The compressible Reynolds equation, which governs the pressure distribution between the slider and the disk can be written as

$$\frac{\partial}{\partial x}\left[ph^3\frac{\partial p}{\partial x}\right]+\frac{\partial}{\partial y}\left[ph^3\frac{\partial p}{\partial y}\right]=6U\mu\frac{\partial}{\partial x}[ph]+6V\mu\frac{\partial}{\partial y}[ph]+12\mu\frac{\partial}{\partial t}[ph] \quad (1)$$

where p is pressure, h is the local slider-disk separation, μ is the viscosity of the air; U and V are the sliding velocities in the x and y directions. This equation is derived by assuming negligible

inertial and body forces, larninar flow, Newtonian viscosity, no-slip boundary conditions at the walls, and small film thickness.

Even though the Reynolds equation is based on the assumption of small film thickness, when the air bearing separation is very small, i.e., on the order of the mean free path of the gas molecules, which is very common in today's magnetic recording applications, the no-slip boundary condition at the wall is no longer satisfied. Then the Reynolds equation should be modified to accommodate the slip flow. There are various molecular slip modification models. The Fukui-Kaneko model (Fukui and Kaneko, 1988) is employed in this study for the ultra-low fly height application. In this model, the modification of the Reynolds equation is based on the linearized Boltzmann equation, and the Poiseule- and Couette-like flows are formulated for arbitrary bearing spacing. If we define the following non-dimensionalized variables

$$X = \frac{x}{L}, Y = \frac{y}{L}, H = \frac{h}{h_m}, P = \frac{p}{p_a}, T = \omega t$$

where L, h,, p_a, ω are the slider's length, minimum spacing, ambient pressure, and appropriate angular frequency, then the generalized form of the Reynolds equation can be written as (Ruiz and Bogy, 1990)

$$\frac{\partial}{\partial X}\left[\hat{Q}PH^3\frac{\partial P}{\partial X} - \Lambda_x PH\right] + \frac{\partial}{\partial Y}\left[\hat{Q}PH^3\frac{\partial P}{\partial Y} - \Lambda_y PH\right] = \sigma\frac{\partial}{\partial T}[PH] \qquad (2)$$

where A, = $6\mu UL/p_a h_m^2$ and $\Lambda_y = 6\mu VL/p_a h_m^2$ are the bearing numbers in the x and y directions, and $\sigma = 12\mu\omega L^2/p_a h_m^2$ is the squeeze number. $\hat{Q}$ is the Poiseuille flow factor, which reflects the type of slip-flow modification used. For the Fukui-Kaneko model, $\hat{Q}$ has the following expression

$$\hat{Q} = f\left(\frac{K_n}{PH}\right)$$

where $K_n = \lambda/h_m$ is the Knudsen number, λ is the mean free path of the gas molecules. $f(K_n/PH)$ is as given by Fukui and Kaneko (1988).

The time-dependent generalized Reynolds equation is discretized using Patankar's control volume method (Patankar, 1980; Cha and Bogy, 1995), in which the unsteady term is discretized

in the implicit form. To improve the efficiency of solution, the final discretization equations are solved using the alternating direction line sweep method combined with a multi-grid method (Hutchinson and Raithby, 1986). Compared with conventional single-grid methods, the multi-grid methods solve the equations on a hierarchy of grids so that all frequency components of the error are reduced at comparable rates (Lu and Bogy, 1994). Inexpensive iteration on the coarse grid rapidly diminishes exactly those components of the error that are so difficult and expensive to reduce by fine grid iteration alone. This results in a dramatic reduction of solution time, especially for the dynamic simulation, since it involves repeated solutions of the discretized Reynolds equation.

2.2 **Dynamics of the Slider.** The two-dimensional equations of motion of the air bearing slider flying in partial contact over a rotating disk are

$$
\begin{aligned}
m\frac{d^2z}{dt^2} &= F_s + F_c + \int_A (p - p_a)\,dA \\
I_\theta\frac{d^2\theta}{dt^2} &= M_{s\theta} + M_{c\theta} + \int_A (p - p_a)(x_g - x)\,dA \\
I_\phi\frac{d^2\phi}{dt^2} &= M_{s\phi} + M_{c\phi} + \int_A (p - p_a)(y_g - y)\,dA
\end{aligned}
\qquad (3)
$$

where z is the vertical displacement, and θ and ϕ are pitch and roll angles, m is the slider's mass, I, and I_ϕ are the slider's moments of inertia, x_g and y_g are the positions of the slider's center of gravity. $F_s, M_{s\theta}$ and $M_{s\phi}$ are the force and moments exerted by the suspension. Similarly, $F_c, M_{c\theta}$ and $M_{c\phi}$ are the total contact force and moments exerted by the disk on the slider.

Dynamic analysis of a slider flying over a rotating disk requires simultaneous solution of the generalized Reynolds equation and the equation of motion of the slider and its suspension. When the slider is disturbed from its steady state flying conditions, the suspension applies time-dependent loading force and moments to the slider. Thus the slider's motion is determined by the balance of the air bearing pressure, the suspension force, the contact forces and the inertia. The suspension force can be represented using either the flexure stiffness and damping coefficients or the suspension dynamics. One efficient approach for integrating the suspension dynamics into the

air bearing simulator is to use modal analysis (Cha and Bogy, 1995). The eigenvalue solution of the suspension is first sought using the commercial FE code ABAQUS, then the dynamic response of the suspension assembly is represented by a truncated linear combination of mode shapes.

Equation (3) is solved using direct numerical integration. The Newmark-β method is implemented in the numerical simulator for high accuracy and less frequency distortion as compared to other commonly used methods. The numerical integration of the coupled equations begins with the estimated displacements of the slider based on the velocities of the previous time step. Then the new displacements are calculated by considering the air bearing pressure and suspension forces at that configuration. These new displacements are compared with the results of the previous iteration step. The iteration ends when the maximum relative change of displacements is smaller than a certain number, which, then gives the final actual displacements of the slider at that time step.

2.3 **Slider/Disk Contact Mechanics.** The contact stresses are assumed to depend on the relative profile of the two surfaces in contact, i.e., upon the shape of the gap between them before loading. The system may then be replaced by a flat, rigid surface in contact with a body having a composite modulus and a profile which results in the same undeformed gap between the surfaces. The elastic-plastic asperity-based contact model (Chang, et al., 1987) is employed to extract the contact forces and moments. It is a probabilistic model. The rough surface is represented by a collection of asperities. The assumptions used in this model are: (1) the rough surface is isotropic; (2) asperities are spherical near their summits; (3) all asperity summits have the same radius R before contact, but their heights vary randomly; (4) asperities are far apart and there is no interaction between them; (5) there is no bulk deformation and only the asperities deform during contact. Besides assuming that the contacting asperities deform elastically according to Hertz's theory (Johnson **1985),** the elastic-plastic model requires volume conservation of a certain control volume of plastically deformed asperities. The friction force is assumed to follow Coulomb's law; the product of the normal contact force and a friction coefficient γ. Let h(x,y)

denote the slider/disk separation at (x,y), and let η denote the area1 density of asperities. The contact force and moments are (see Chang, et al., 1987, for more details)

$$F_c = \eta E \iint_A \left\{ \frac{4}{3} R^{1/2} \int_h^{h+\delta_c} (\xi - h)^{3/2} \varphi(\xi) d\xi + \pi RK \frac{Y}{E} \int_{h+\delta_c}^{\infty} [2(\xi - h) - \delta_c] \varphi(\xi) d\xi \right\} dA$$

$$M_{c\theta} = \eta E \iint_A \left\{ (x - x_g) \left[\frac{4}{3} R^{1/2} \int_h^{h+\delta_c} (\xi - h)^{3/2} \varphi(\xi) d\xi + \pi RK \frac{Y}{E} \int_{h+\delta_c}^{\infty} [2(\xi - h) - \delta_c] \varphi(\xi) d\xi \right] + h_{cg} \gamma \left[\frac{4}{3} R^{1/2} \int_h^{h+\delta_c} (\xi - h)^{3/2} \varphi(\xi) d\xi + \pi RK \frac{Y}{E} \int_{h+\delta_c}^{\infty} [2(\xi - h) - \delta_c] \varphi(\xi) d\xi \right] \cos\psi \right\} dA$$

$$M_{c\phi} = \eta E \iint_A \left\{ (y - y_g) \left[\frac{4}{3} R^{1/2} \int_h^{h+\delta_c} (\xi - h)^{3/2} \varphi(\xi) d\xi + \pi RK \frac{Y}{E} \int_{h+\delta_c}^{\infty} [2(\xi - h) - \delta_c] \varphi(\xi) d\xi \right] + h_{cg} \gamma \left[\frac{4}{3} R^{1/2} \int_h^{h+\delta_c} (\xi - h)^{3/2} \varphi(\xi) d\xi + \pi RK \frac{Y}{E} \int_{h+\delta_c}^{\infty} [2(\xi - h) - \delta_c] \varphi(\xi) d\xi \right] \sin\psi \right\} dA \qquad (4)$$

where ψ is the skew angle, x_g and y_g are the coordinates of the slider's gravity center, and h_{cg} is the vertical distance between the point (x,y) and the center point of gravity. The critical interference, δ_c, at which onset of plastic deformation occurs is

$$\delta_c = \left(\frac{\pi KY}{2E} \right)^2 R$$

where E is the composite Young's modulus, Y is the yield strength and K is the yield coefficient, which is a function of Poisson's ratio. $\varphi(\xi)$ is the asperity height distribution function. In our study, a Gaussian probability distribution is assumed

$$\varphi(\xi) = \frac{1}{\sqrt{2\pi}\sigma} \exp\left(-\xi^2 / 2\sigma^2\right),$$

where σ is the standard deviation of the asperity heights.

During the simulation, the program computes at each time step the expected values of the normal contact force, the contact moments and the friction force based on the film thickness distribution. These forces and moments are then used to calculate the motion of the slider.

3 Results and Discussions

The "Nutcracker" slider designed in CML and built by Read-Rite Corporation is used for the sample calculations. It is a shaped-rail 50% sub-ambient pressure type slider. Figure 1 shows the shape of its air bearing surface. The slider has a 24 degrees wall angle from horizontal. The

design target fly height is about 25 nm under 3.5 grams of suspension load. The slider design has a center rail that carries the read-write element. The read-write point is offset 25 μm forward from the trailing edge. The slider used in our calculations is assumed to have a 15nm crown. It is also designed with a positive 10nm camber so that the closest point of separation with the disk is near the center rail trailing edge. The rail shapes are concave on both sides to minimize the fly height change across the disk. The connected front region of the air bearing surfaces enables the efficient generation of the sub-ambient pressure in the central recessed regions. The disk rotational speed is 5400 rpm. In our simulation, the Hutchinson 1650E type suspension is used. Its FEM mesh is displayed in Fig. 2. 333 1 nodes are used to model this suspension with a dense mesh distribution in the portion of the integrated gimbal. The eigenvalue solution is first obtained using ABAQUS, then the first 10 modes are used in the air bearing simulation to represent the suspension dynamics during the take-off event.

Figures 3 and 4 show the slider's contact take-off dynamics during the early moments of the start-up through the first 16 ms. As seen in Fig. 3, the slider is initially at rest on the disk surface, when at 0.01 ms, the disk begins to rotate. Due to the positive crown and the sudden action of the contact friction force at the interface, the slider oscillates mainly in the pitch mode for about 0.1 ms. After the initial transient oscillation, the slider's pitch decreases under the contact friction force at the interface, resulting in an increase in the trailing edge fly height. As shown in Fig. 4, the trailing edge fly height reaches a maximum of 15.2 nm at about 1.5 ms, and then decreases as the disk speed is increasing. Figure 5 shows the continuation of the flying characteristics as functions of the disk speed after the start-up. As the disk speed increases, the air bearing pressure builds up in the front taper region, increasing the pitch of the slider. The trailing edge fly height thus decreases, attaining a minimum of 5.1 nm at the disk speed of 0.44 m/s, which is well below the at-rest spacing, and then it increases with the disk speed as it takes off. The disk velocity at which the slider takes off from the disk is referred to as the take-off velocity (TOV) of the slider. The practice of using a given fly height to determine the TOV assumes that the take-off fly height is independent of the air bearing and other design parameters.

This assumption does not reflect the slider/disk contact conditions during the take-off process. It will be shown later that the take-off fly height, just like the TOV, depends on many air bearing and other design parameters. The more physically realistic criterion for determinmg the process of a slider taking off from a disk is a pre-defined contact force as a percent of the preload. Throughout this study, it is assumed that take-off from a disk takes place at the disk speed at which the normal contact force reduces to only 1% of the preload. The fly height at the read-write point at take-off is referred to as the take-off fly height. Using this definition, we calculated the TOV and the take-off fly height for the case shown in Figs. 3,4 and 5. The slider takes off at a TOV of 0.98 m/s and the take-off fly height at the read-write point is 7.1 nm.

3.1 Effect of Slider Crown. The crown is a longitudinal parabolic surface superimposed lengthwise on the slider's ABS. Figure 6 shows the TOV as a function of crown height. As expected, the larger crown sliders take off faster (at a lower disk velocity) than sliders with smaller crown. The plot also shows that the decrease in the TOV is nonlinear in the range from 0 to 30 nm. The rate of TOV decrease with crown drops rapidly as the crown increases. At the higher crown heights, the crown effect on the TOV is less. This agrees with results obtained by Bolasna (1990). Figure 7 shows that the take-off fly height increases with the crown height. The effect of crown on the initial flying characteristics during the contact start-up are shown in Fig. 8. The trailing edge fly height and pitch changes from the at-rest values for the slider with two different crown heights are plotted. The slider with 30nm crown experiences a much larger amplitude transient oscillation and has a greater pitch drop than the slider without crown.

3.2 Effect of Slider Camber. The camber is a deviation from flatness of the ABS similar to crown, except that it is in the transverse direction. Figure 9 is a plot of the TOV versus camber heights from 5 nm to 25 nm. The TOV increases almost linearly with camber height at a rate of about 0.034 m/s/nm, while the take-off fly height decreases as camber height increases (Fig. 10). During the contact start-up, an increase of the camber height reduces slightly the amplitudes of the transient flying height and pitch oscillations from their static values as shown in Fig. 11.

3.3 Effect of Slider Twist. The twist is given in terms of the relative height of four corners to the center. A positive twist increases the separation between the slider and the disk at the inner leading edge and the outer trailing edge, and decreases the separation at the outer leading edge and inner trailing edge. Figure 12 shows the TOV as a function of the twist. The effect of twist on the TOV is smaller than the crown and camber. The TOV decreases nearly linearly as the twist changes from -10 nm to 10 nm. The take-off fly height does not appear to change much with twist, as illustrated in Fig 13. Figure 14 shows the transient oscillations from rest values of the trailing edge fly height and pitch during the contact start-up for twist values of 0 and 5 nm. The slider with larger twist has less initial pitch drop.

3.4 **Effect of Slider Taper Angle. In** this study, the taper length is kept constant, and different taper angles are achieved through changing the taper height at the leading edge. Figure 15 shows the TOV versus taper angle. The corresponding take-off fly height is plotted in Fig. 16. The sliders with smaller taper angle take off at a lower disk velocity and a lower take-off fly height than the sliders with larger taper angle. This is because a smaller taper angle improves the generation of the air bearing pressure in the front taper region during the take-off stage. As the taper angle increases, the rate of change of the TOV decreases. During the initial contact start-up, the larger taper angle sliders have a smaller increase of trailing edge fly height than the smaller taper angle sliders as shown in Fig. 17.

3.5 **Effect of Disk Surface Roughness.** Figure 18 shows the TOV as a function of the standard deviation of the asperity heights (σ). As expected, the sliders take off at higher TOV's from rougher disk surfaces than from smoother disk surfaces. The rate of change of the TOV increases as σ increases. The take-off fly height increases linearly with σ (Fig. 19). Figure 20 illustrates the initial transient flying characteristics during the contact start-up for σ=3 nm and 6 nm. When taking off from a rougher disk surface, the sliders endure a larger amplitude and slower decaying oscillation. The rougher disk surface also results in a higher increase of the trailing edge fly height.

3.6 Effect of Friction Coefficient. Figures 21 and 22 show the TOV and the take-off fly height versus the friction coefficient, respectively. It is seen that the friction coefficient does not have any influence on the TOV. The only noticeable effect is a slight increase of the take-off fly height with the friction coefficient. Even though the friction coefficient has the least effect on the TOV and the take-off fly height, it has a substantial influence on the initial flying characteristics during the start-up, as shown in Fig. 23. The larger friction coefficient introduces a larger amplitude and slower decaying oscillation. This is expected since the contact start-up oscillation is mainly generated by the sudden action of the friction force at the interface at start-up. The increase of the trailing edge fly height for the friction coefficient of 0.5 is more than twice that for the friction coefficient of 0.2.

4 Conclusions

A mixed lubrication model is developed for investigating various air bearing and other design parameter effects on the slider's take-off performance. The Fukui-Kaneko linearized Boltzmann equation is used to model the nonlinear rarefaction effects in the modified Reynolds equation for fly heights down to contact. An elastic-plastic asperity-based contact model is employed to extract the slider/disk contact forces and moments during the take-off process. The criterion for take-off from a disk is defined as a specified percent of the suspension preload. A sub-25nm slider with shaped-rails is used in this study. The effects of the slider's crown, camber, twist, taper angle, and, the disk surface roughness and friction coefficient on the take-off velocity and the take-off fly height, as well as the transient flying characteristics during start-up, are studied. Among the many air bearing and other design parameters affecting the take-off velocity, the slider's crown and disk surface roughness are particularly important. Larger crowns and smoother disk surfaces reduce the take-off velocity, The contact start-up take-off flying characteristics are mostly affected by the slider's crown and the contact friction coefficient. Smaller crowns and friction coefficients produce a smoother initial take-off performance.

Acknowledgments

This study is supported by the Computer Mechanics Laboratory at the University of California at Berkeley. We would like to thank Ryan Jurgenson of Hutchinson Technology for providing us the FEM mesh of the suspension.

References

Bolasna, S., 1990, "Air Bearing Parameter Effects on Take-off Velocity," ***IEEE Transactions on Magnetics,*** Vol. 26, No. 6, pp.3003-3038

Cha, E., and Bogy, D. B., 1995, "A Numerical Scheme for Static and Dynamic Simulation of Subambient Pressure Shaped Rail Sliders," ***ASME Journal of Tribology,*** Vol. 117, pp.36-46.

Chang, W. R., Etsion, I., and Bogy, D. B., 1987, "An Elastic-Plastic Model for the Contact of Rough Surfaces," ***ASME Journal of Tribology,*** Vol. 109, pp.257-263.

Fukui, S., and Kaneko, R., 1988, "Analysis of Ultra-Thin Gas Film Lubrication Based on Linearized Boltzmann Equation: First Report-Derivation of a generalized Lubrication Equation Including Thermal Creep Flow," ***ASME Journal of Tribology*** , Vol. 110, pp.335-341.

Hutchinson, B. R., and Raithby, G. D., 1986, "A Multigrid Method Based on the Additive Correction Strategy," ***Numerical Heat Transfer,*** Vol. 9, pp.5 1 l-537.

Johnson, K. L., 1985, "Contact Mechanics," Cambridge University Press, Cambridge.

Lee, H. J., Hempstead, R. D., and Weiss, J., 1989, "Study of Head and Disk Interface in Contact Start Stop Test," ***IEEE Transactions on Magnetics,*** Vol. 25, No. 5, pp.2748-2750.

Lu, S., and Bogy, D. B., 1994, "A Multi-Grid Control Volume Method for the Simulation of Arbitrarily Shaped Slider Air Bearing with Multiple Recess Levels," ***Technical Report No. 94-016,*** Computer Mechanics Laboratory, U. C. Berkeley.

Patankar, S. V., 1980," ***Numerical Heat Transfer and Fluid Flow,"*** McGraw-Hill.

Ruiz, 0. J., and Bogy, D. B., 1990, "A Numerical Simulation of the Head-Disk Assembly in Magnetic Hard Disk: 1. Component Models," ***ASME Journal of Tribology,*** Vol. 112, pp.593-602.

Suk, M., Ishii, T. **,** and Bogy, D. B., 1992, "The Influence of Air-Bearing Surface Geometry on the Dynamics of Sliders," ***ASME Journal of Tribology,*** Vol. 114, pp.26-3 1.

Zhu, L. Y., and Bogy, D. B., 1989, "A Multi-channel Laser Interferometer and its Use to Study Head-Disk Interface Dynamics in Magnetic Disk Drives," ***Tribology and Mechanics of Magnetic Storage Systems,*** STLE Vol. VI, pp. 168-179.

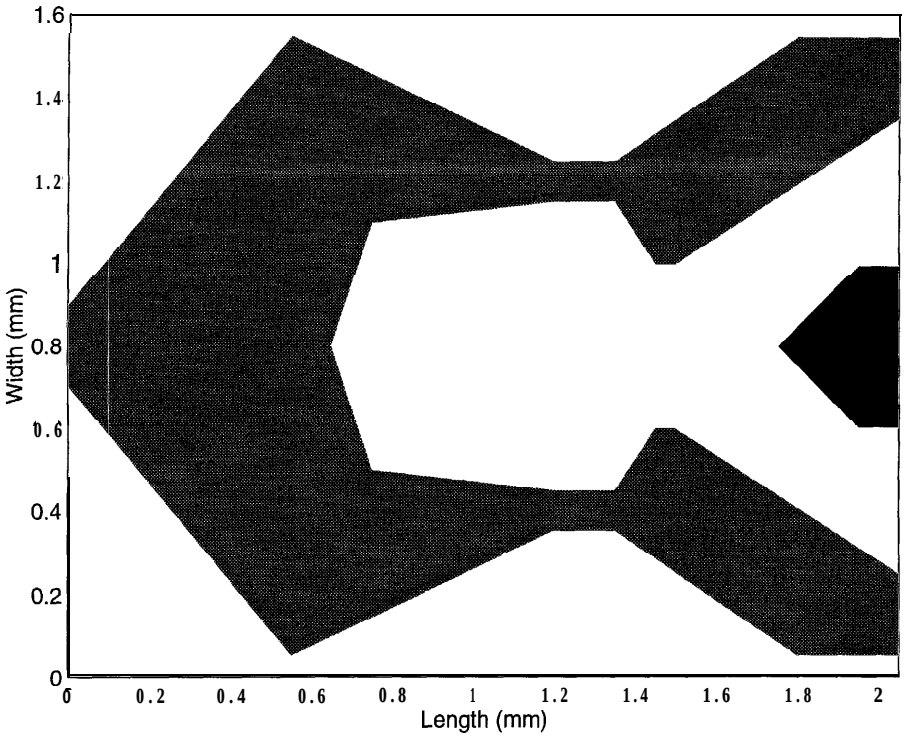

Fig. 1 Air bearing surface for the Nutcracker slider

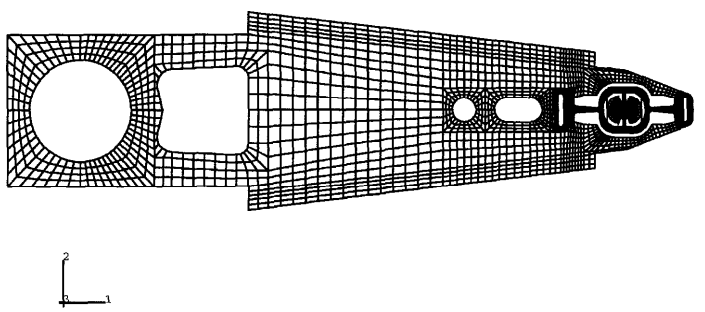

Fig. 2 FEM mesh of a Hutchinson 165OE type suspension

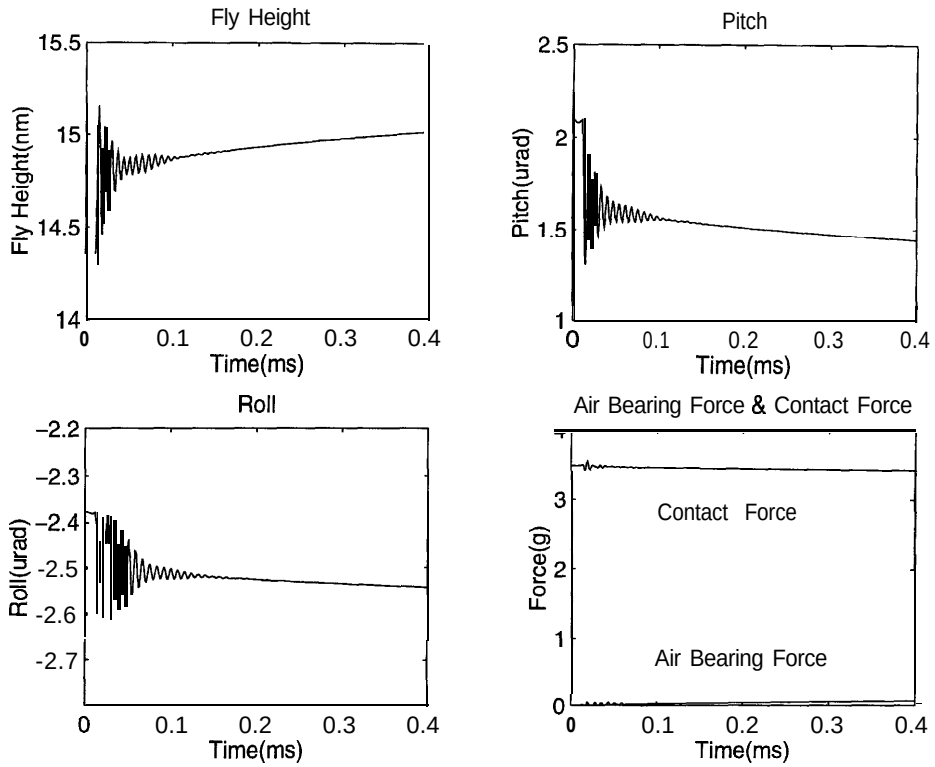

Fig. 3 Flying characteristics during the contact start-up (up to the disk speed of 0.0018 m/s).

Crown = 15 nm, camber = 10 nm, twist = 0, taper angle = 0.01 rad, $\gamma = 0.2$ and $\sigma = 3$ nm

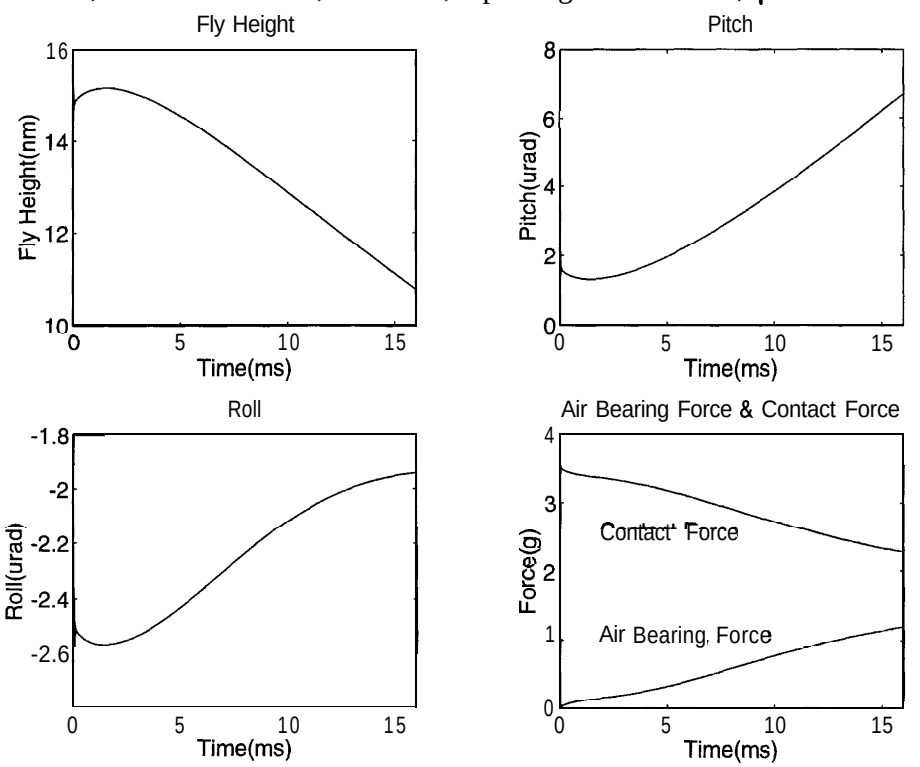

Fig. 4 Flying characteristics during the contact start-up (up to the disk speed of 0.072 m/s).
Crown = 15 nm, camber = 10 nm, twist = 0, taper angle = 0.01 rad, $\gamma = 0.2$ and $\sigma = 3$ nm

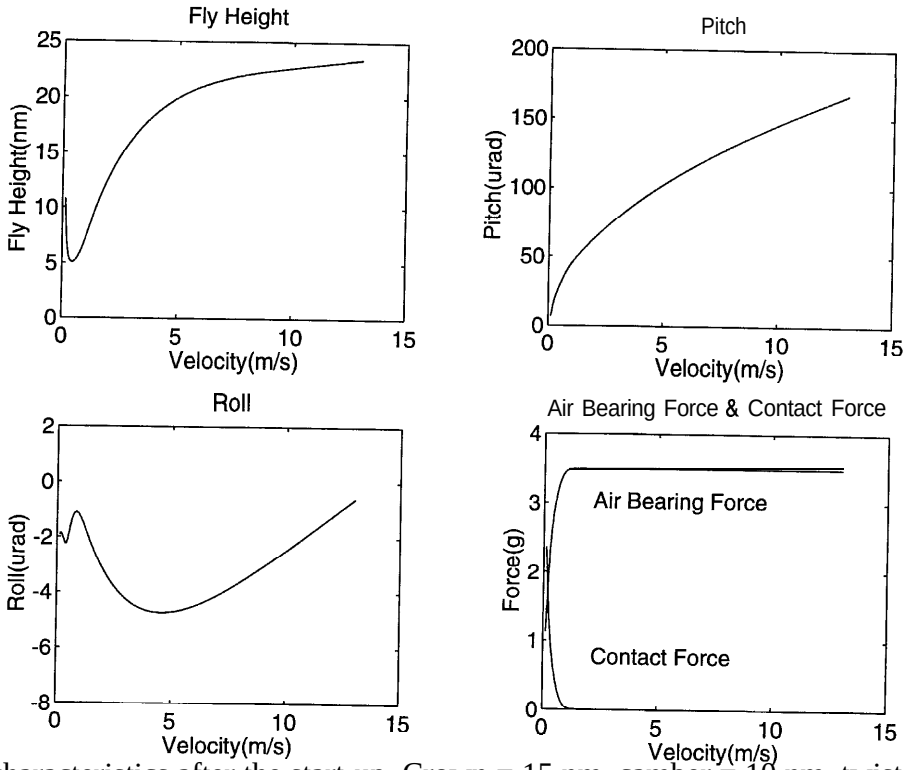

Fig. 5 Fly characteristics after the start-up. Crown = 15 nm, camber = 10 nm, twist = 0, taper angle = 0.01 rad, $\gamma = 0.2$ and $\sigma = 3$ nm

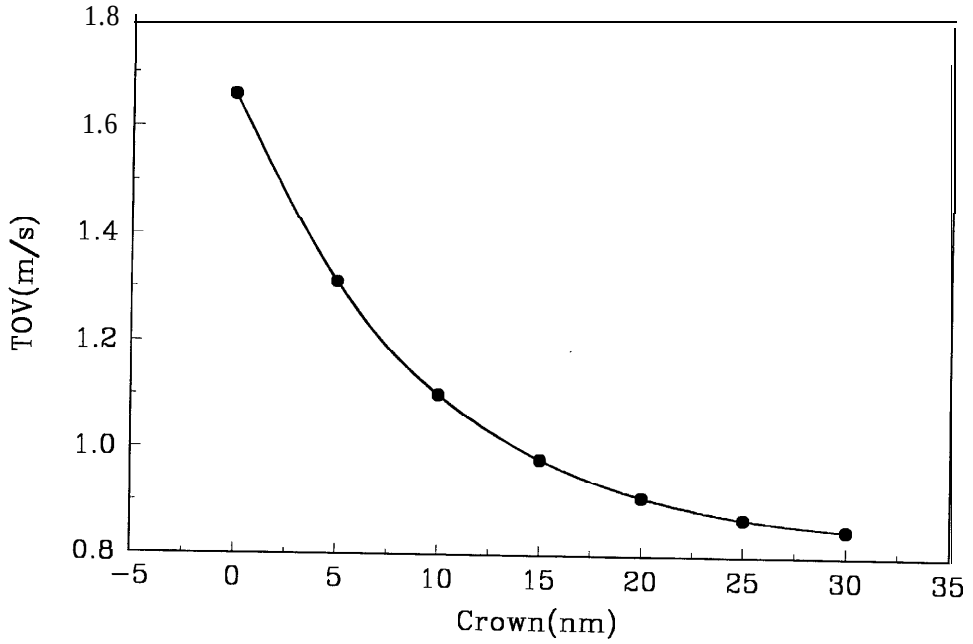

Fig. 6 Take-off velocity versus crown. Camber = 10nm, twist = 0, taper angle = 0.01 rad, $\gamma = 0.2$ and $\sigma = 3$nm

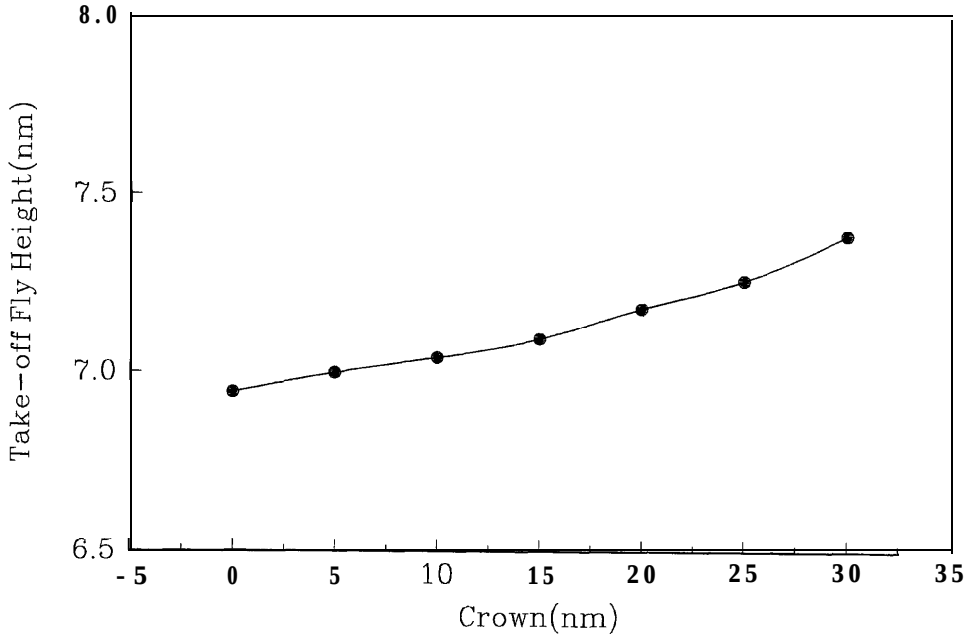

Fig. 7 Take-off fly height versus crown. Camber = 10nm, twist = 0, taper angle = 0.01 rad, γ = 0.2 and σ = 3nm

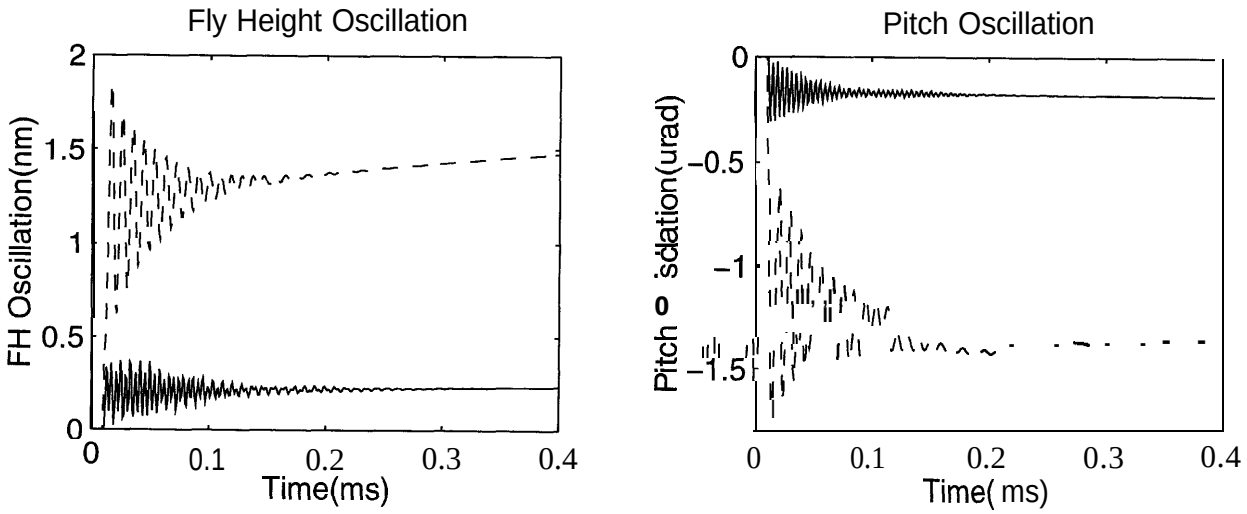

Fig. 8 Fly height and pitch oscillations during the contact start-up for two crown heights. Crown = Onm (solid lines) and crown = 30nm (dash lines)

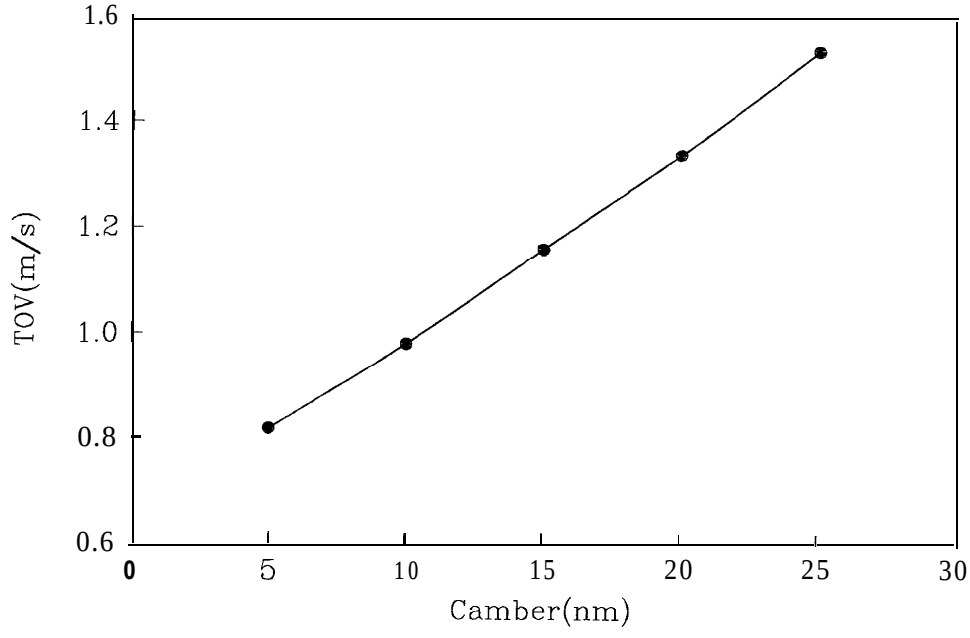

Fig. 9 Take-off velocity versus camber. Crown = 15nm, twist = 0, taper angle = O.Olrad, γ = 0.2 and σ = 3nm

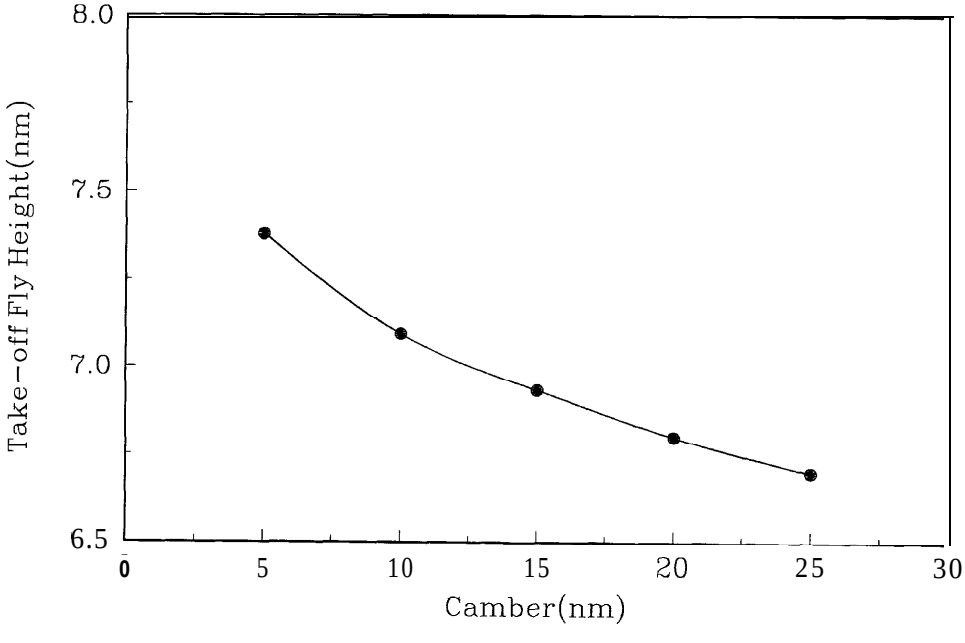

Fig. 10 Take-off fly height versus camber. Crown = 15nm, twist = 0, taper angle = O.Olrad, γ = 0.2 and σ = 3nm

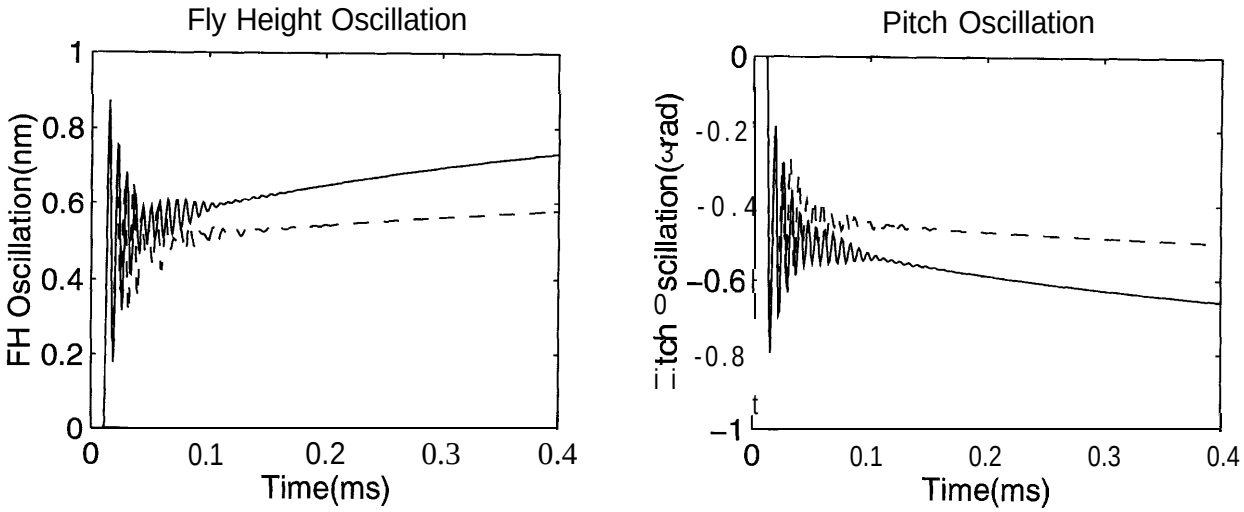

Fig. 11 Fly height and pitch oscillations during the contact start-up for two camber heights. Camber = 10nm (solid lines) and camber = 20nm (dash lines)

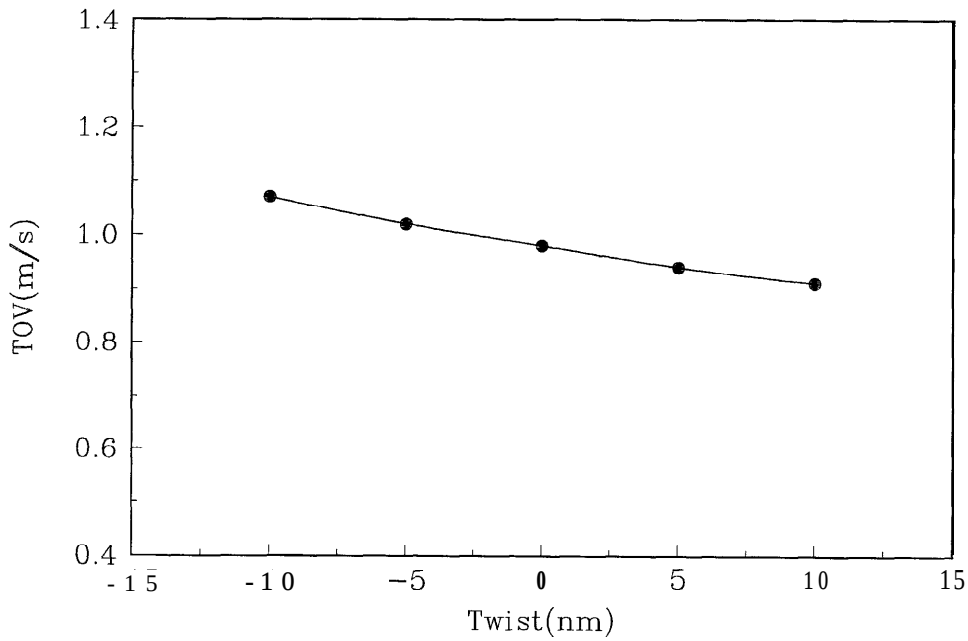

Fig. 12 Take-off velocity versus twist. Crown = 15nm, camber = 10nm, taper angle = 0.01rad, γ = 0.2 and σ = 3nm

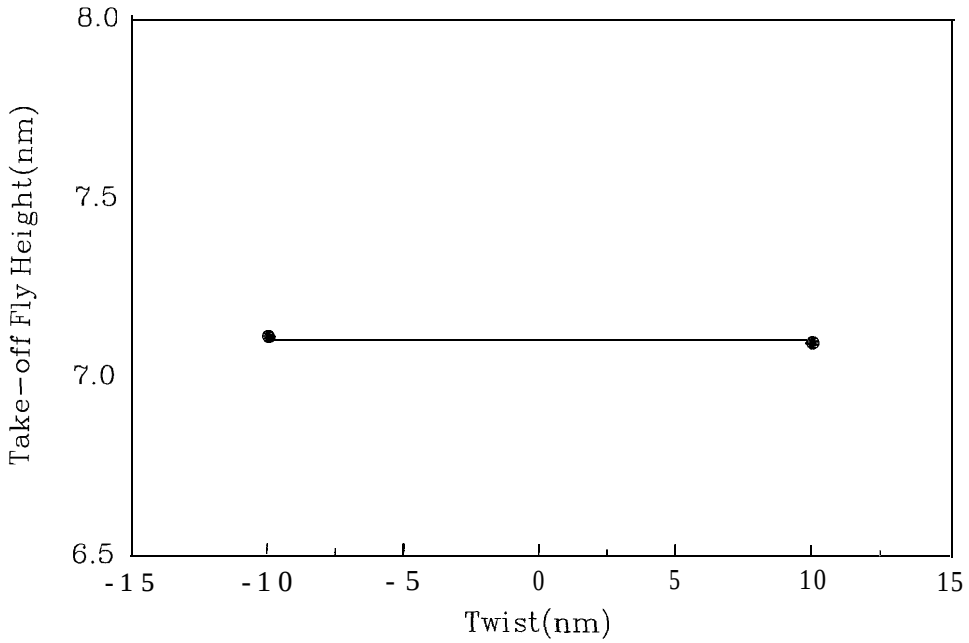

Fig. 13 Take-off fly height versus twist. Crown = 15nm, camber = 10nm, taper angle = O.Olrad, γ = 0.2 and σ = 3nm

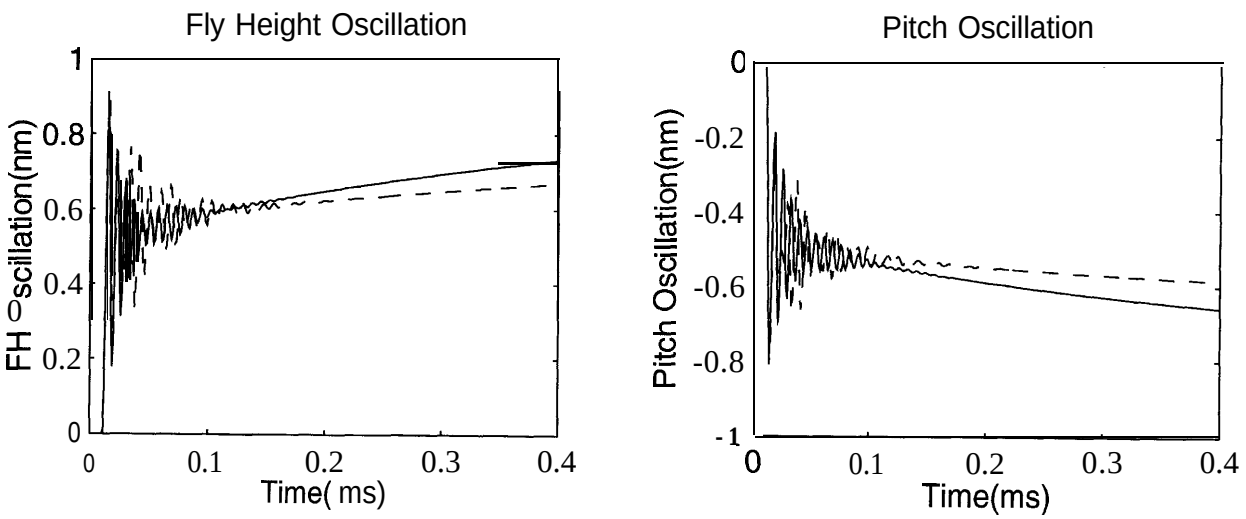

Fig. 14 Fly height and pitch oscillations during the contact start-up for two twist values. Twist = Onm (solid lines) and twist = 5nm (dash lines)

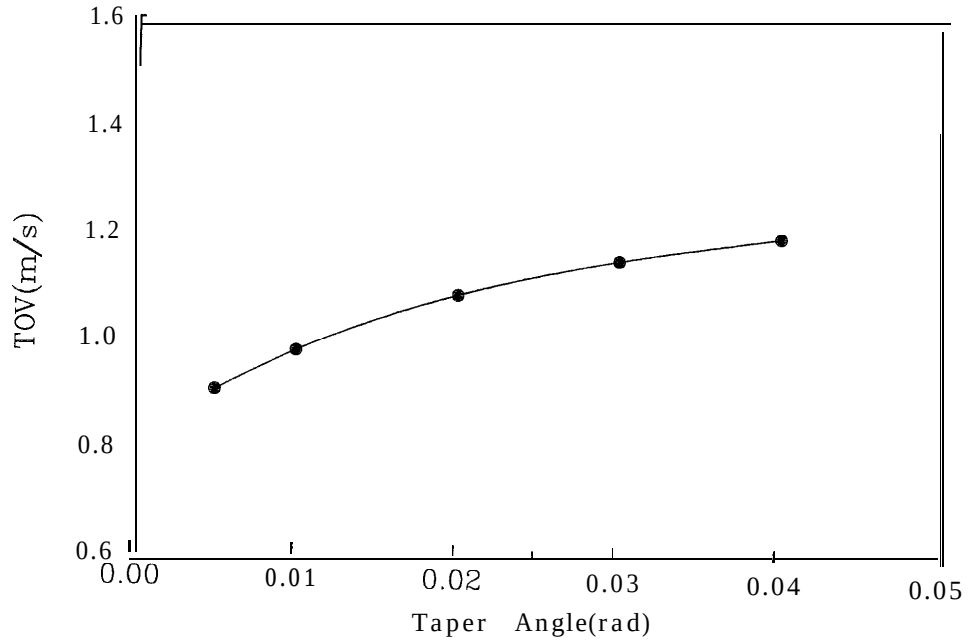

Fig. 15 Take-off velocity versus taper angle. Crown = 15nm, camber = 10nm, twist = 0 γ = 0 2 and σ = 3nm

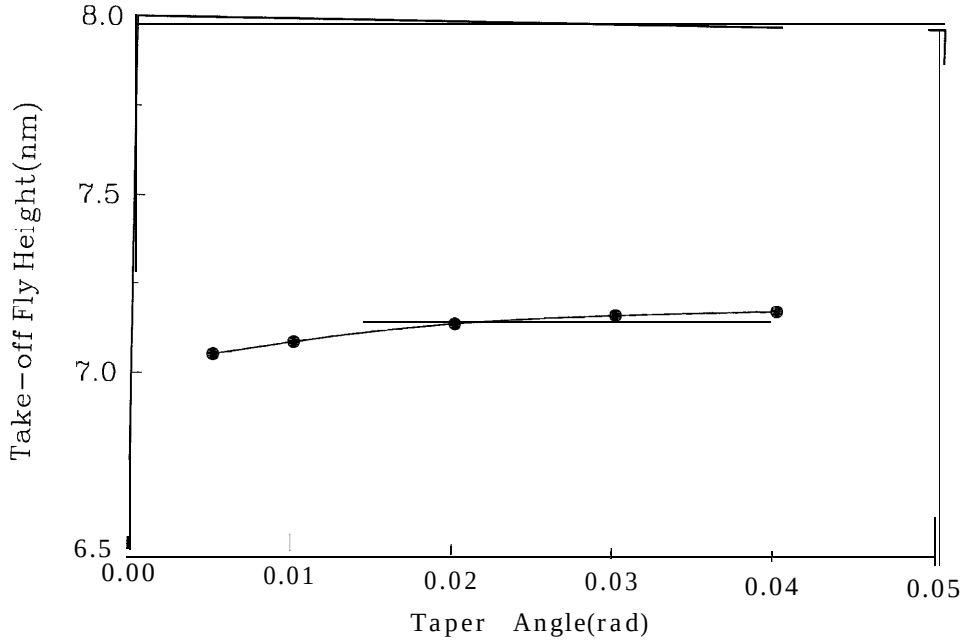

Fig. 16 Take-off fly height versus taper angle. Crown = 15nm, camber = 10nm, twist = 0 γ = 0 2 and σ = 3nm

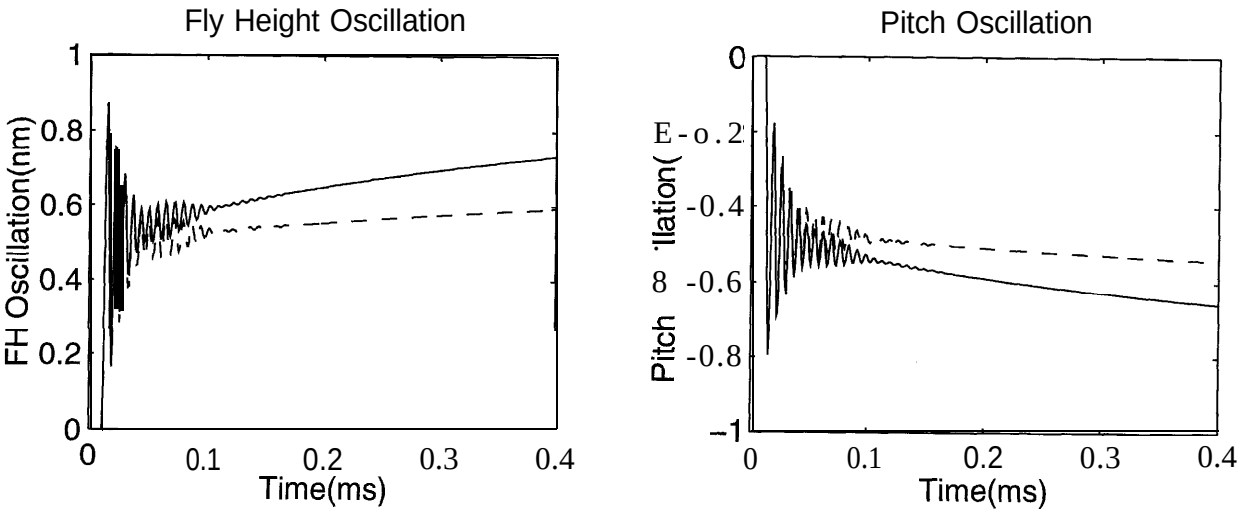

Fig. 17 Fly height and pitch oscillations during the contact start-up for two taper angles. Taper angle = 0.01 rad (solid lines) and taper angle = 0.02 rad (dash lines)

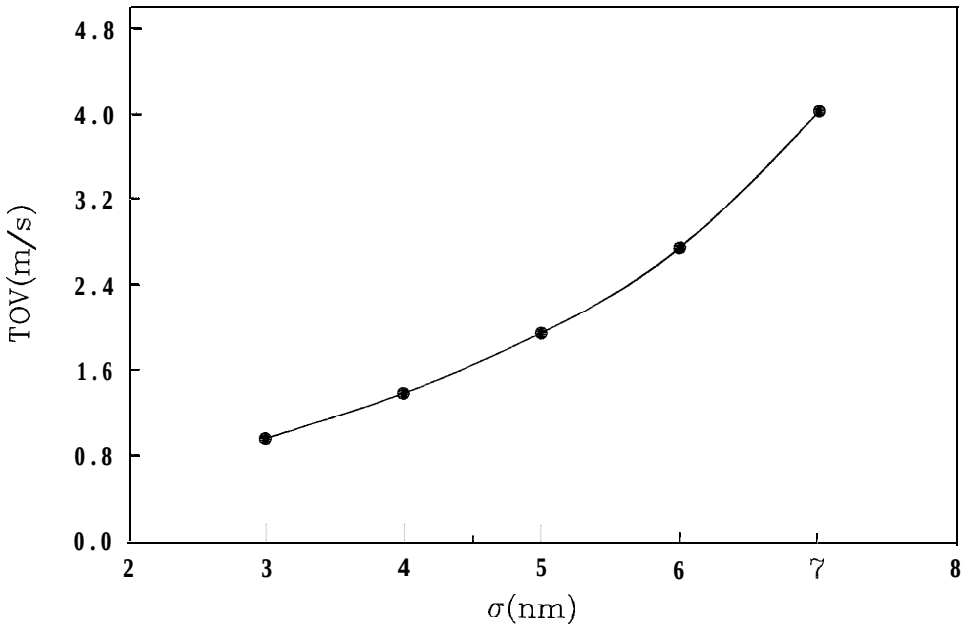

Fig. 18 Take-off velocity versus the standard deviation of surface roughness. Crown = 15nm, camber = 10nm, twist = 0, taper angle = O.Olrad, and $\gamma = 0.2$

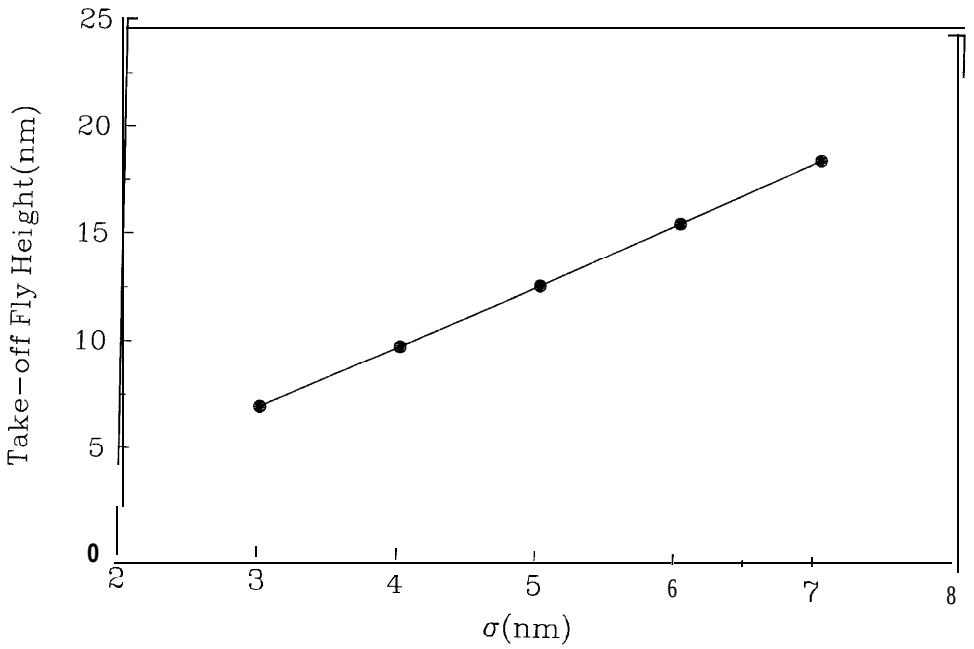

Fig. 19 Take-off fly height versus the standard deviation of surface roughness. Crown = 15nm, camber = 10nm, twist = 0, taper angle = O.Olrad, and $\gamma = 0.2$

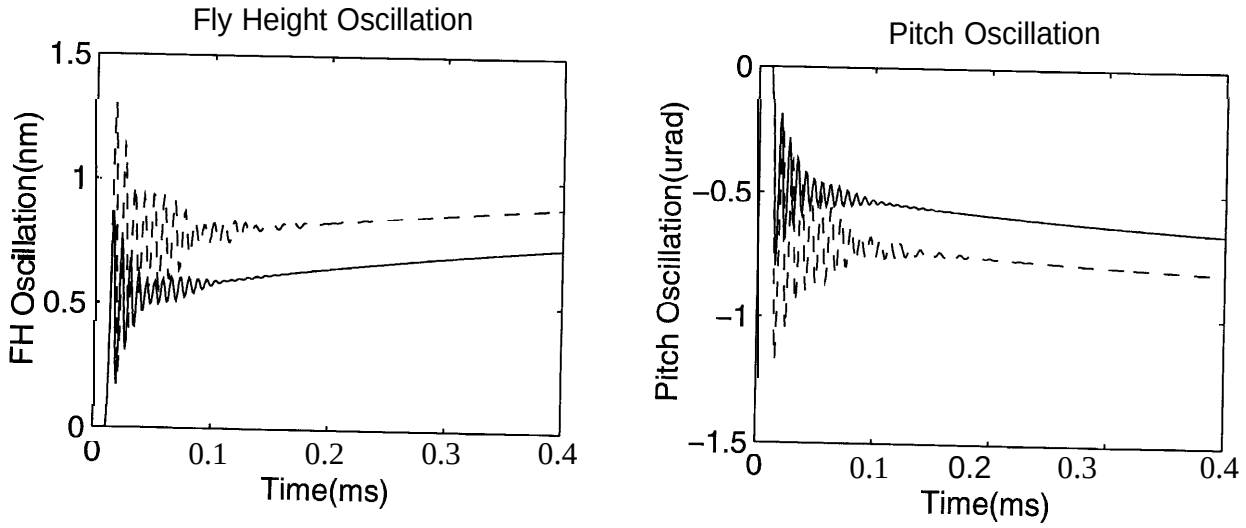

Fig. 20 Fly height and pitch oscillations during the contact start-up for two σ values. σ = 3nm (solid lines) and σ = 6nm (dash lines)

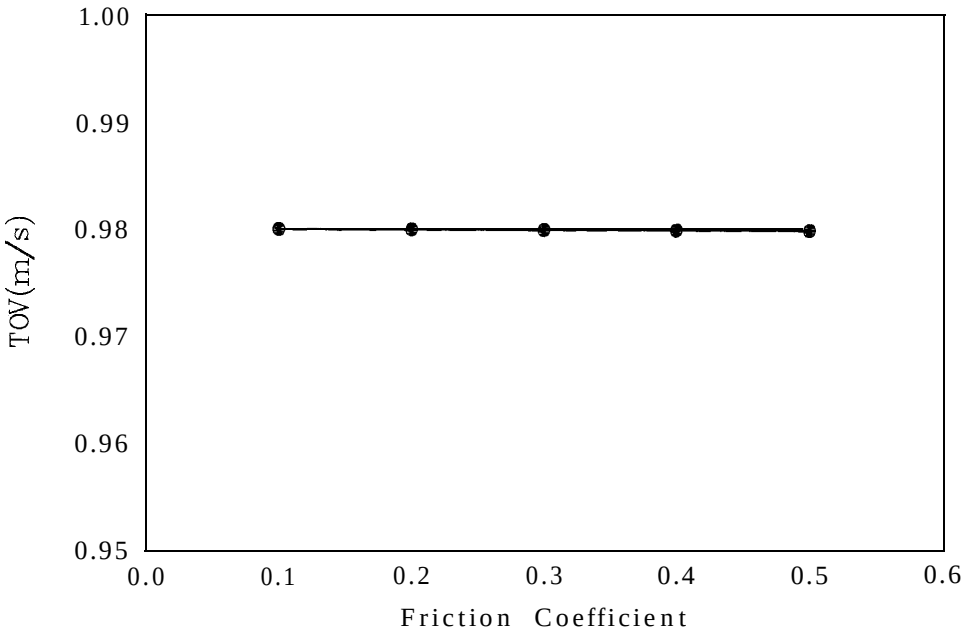

Fig. 21 Take-off velocity versus friction coefficient. Crown = 15nm, camber = 10nm, twist = 0, taper angle = O.Olrad, and σ = 3nm

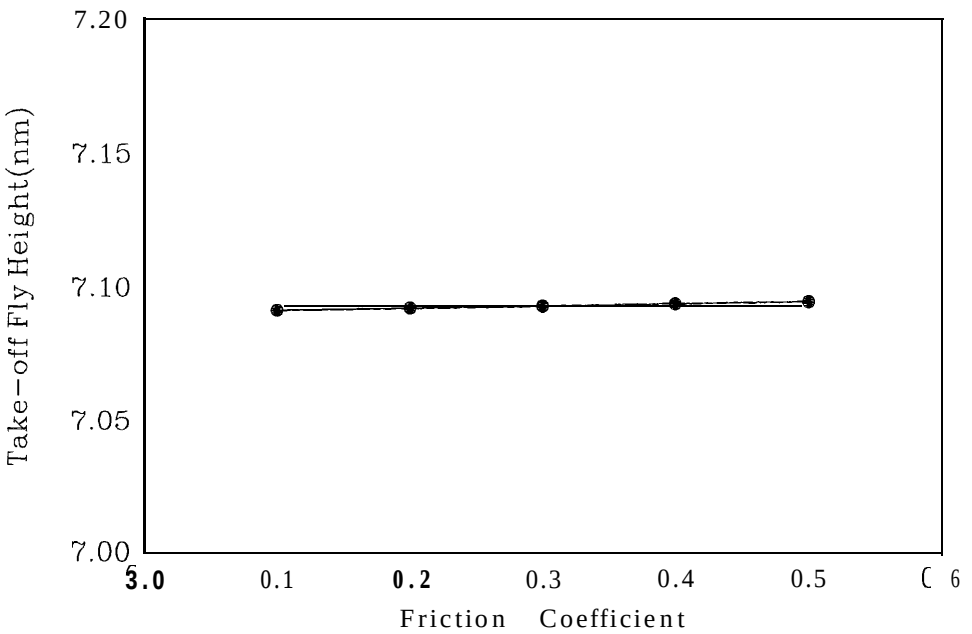

Fig. 22 Take-off fly height versus friction coefficient. Crown = 15nm, camber = 10nm, twist = 0, taper angle = O.Olrad, and σ = 3nm

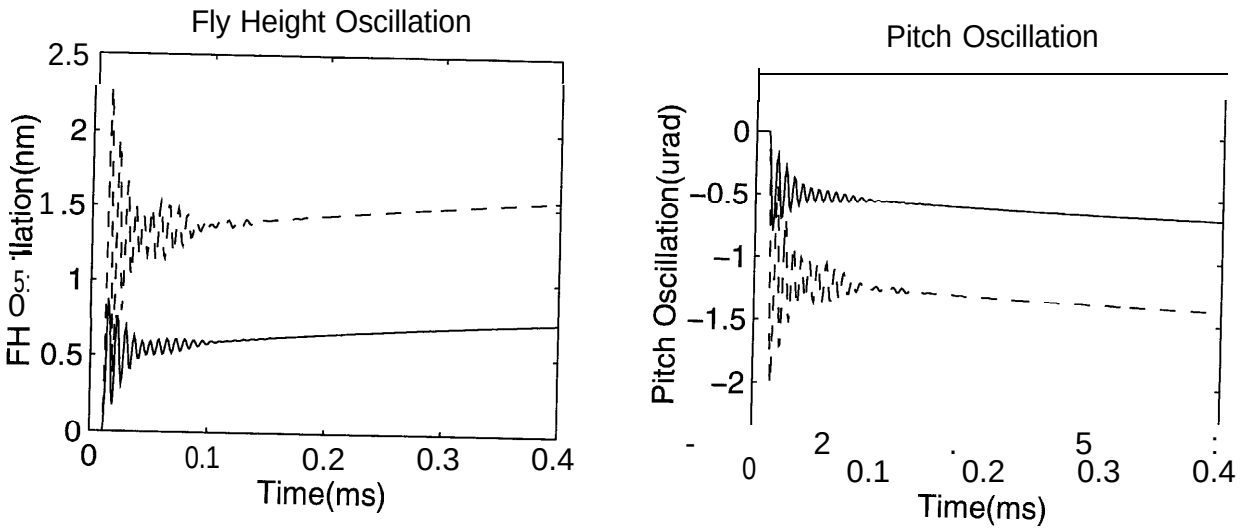

Fig. 23 Fly height and pitch oscillations during the contact start-up for two friction coefficients. γ = 0.2 (solid lines) and γ = 0.5 (dash lines)